Nanoscale

ARTICLE

Field emission and anode etching during formation of length-controlled nanogaps in electrical breakdown of horizontally aligned single-walled carbon nanotubes

Received 00th January 20xx,
Accepted 00th January 20xx

DOI: 10.1039/x0xx00000x

www.rsc.org/

Keigo Otsuka,[a] Taiki Inoue,[*a] Yuki Shimomura,[a] Shohei Chiashi[a] and Shigeo Maruyama[*a,b]

We observe field emission between nanogaps and voltage-driven gap extension of single-walled carbon nanotubes (SWNTs) on substrates during electrical breakdown process. Experimental results show that the gap size is dependent on the applied voltage and humidity, which indicates high controllability of the gap size by appropriate adjustment of these parameters in accordance with the application. We propose a mechanism for the gap formation during electrical breakdown as follows. After small gaps are formed by Joule heating-induced oxidation, SWNTs on the anode side are electrochemically etched due to physically-adsorbed water from the air and the enhanced electric field at the SWNT tips. Field emission is measured in a vacuum as a possible mechanism for charge transfer at SWNT gaps. The relation between the field enhancement factor and geometric features of SWNTs explains both the voltage dependence of the extended gap size and the field emission properties of the SWNT gaps. In addition, the similar field-induced etching can cause damage to adjacent SWNTs, which possibly deteriorates the selectivity for cutting metallic pathways in the presence of water vapor.

Introduction

Electrical breakdown[1] of single-walled carbon nanotubes (single-walled CNTs, SWNTs) has been performed to selectively cut metallic SWNTs (m-SWNTs) for field-effect transistor (FET) applications,[2–5] or to create SWNT nanogaps for use as nanoscale electrodes[6–8] to contact single molecules[9,10] and functional materials.[11] When a high bias voltage is applied across SWNTs, the SWNTs are physically cut at the hottest points due to self-heating-induced oxidation,[12,13] and become electrically insulating due to formation of the gap. Electrical breakdown has been widely applied to both SWNTs on substrates and suspended over trenches[10,14] because it is an extremely simple operation.

However, even limited to individual SWNTs on substrates, the size of nanogaps (L_{gap}) obtained from electrical breakdown vary widely from ca. 2 nm[15] to more than 100 nm.[11] The reason for the wide variation of gap size has not been fully explained, even though the mechanism of gap formation seems simple. Instead, gap formation of multi-walled CNTs (MWNTs) and SWNT bundles has been observed in more detail, despite the more complicated processes involved with the layer-by-layer oxidation of multiple shells.[1,12,16–18] For any application, the gap size has a significant effect on the device performance and should thus be carefully controlled. For example, nanogaps in SWNT array channels of SWNT-FETs amplify and localize the electric field and could result in a correlated breakdown of neighboring SWNTs.[19,20] The extent to which the field is amplified is highly dependent on the nanogap size; therefore, the gap size should be designed in accordance with the device requirements. On the other hand, phase change memory devices that employ SWNTs as electrodes[11] require smaller gaps to achieve higher energy efficiency. There is a lack of detailed understanding on the formation mechanisms of SWNT gaps; however, the controllability of nanogap size has been reported to a limited extent; shorter distance between two metallic contacts (SWNT length or channel length; L_{ch}) or breakdown in Ar gas flow results in smaller nanogaps,[11,15] although there has been little explanation of the reason for the small gap formation.

In this work, we report the voltage-driven gap extension phenomenon of SWNTs after electrical breakdown. It is generally considered that SWNTs cut by electrical breakdown are not conductive due to the physical gaps; therefore, no structural changes are expected for the broken SWNTs by external voltage application. However, we carefully observe field emission current at SWNT gaps and the increased gap size of broken SWNTs by application of a DC voltage. The dependence of the gap size on the applied voltage and ambient humidity was investigated. Based on the experimental results, we consider that electrochemical etching at the SWNT tips due to physisorbed water and enhanced electric field is the driving force behind the gap extension. When it comes to SWNT-FET applications, the voltage-driven SWNT etching may negatively affect the selectivity for breaking metallic pathways because

[a] Department of Mechanical Engineering, The University of Tokyo, Tokyo 113-8656, Japan.
E-mail:; inoue@photon.t.u-tokyo.ac.jp; maruyama@photon.t.u-tokyo.ac.jp
[b] Energy NanoEngineering Lab., National Institute of Advanced Industrial Science and Technology (AIST), Ibaraki 305-8564, Japan.
Electronic Supplementary Information (ESI) available: See DOI: 10.1039/x0xx00000x

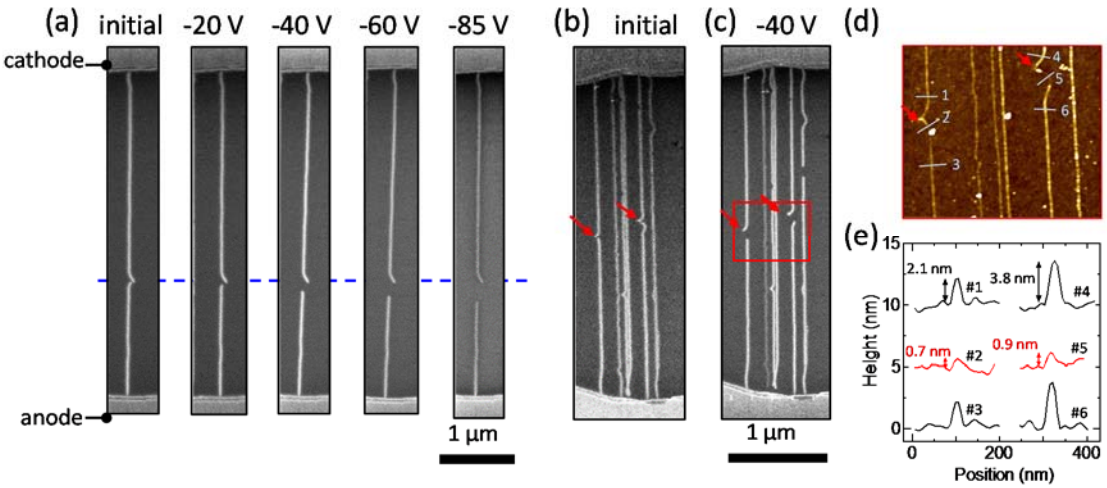

Figure 1 (a) SEM images of an SWNT after gap formation and gap extension in air. The initial gap was formed with a ramp voltage up to V_{max} = 25 V on a heated substrate, followed by subsequent application of V_{max} = 20, 40, 60 and 85 V at room temperature. SEM images of SWNTs (b) after nanogap formation and (c) after gap extension with ramp voltage up to V_{max} = 40 V applied. (d) AFM image of the region outlined in red in (c). The initial gap location is indicated by arrows. (e) Cross-sectional profiles of two sets of SWNTs (black) and gaps (red) at the positions numbered 1 to 6 in (d).

semiconducting SWNTs (s-SWNTs) can be remotely damaged by adjacent nanogaps.

Results and discussion

Voltage-driven gap extension of SWNTs

Electrical breakdown of SWNT arrays (L_{ch} = 5 µm) was performed in air with a ramping voltage from 0 to -25 V at ca. 100 °C. A positive gate voltage (V_G = +10 V) was applied to break only m-SWNTs. Figure 1 shows scanning electron microscopy (SEM) images of a typical SWNT gap. After gap formation, ramp voltages from 0 to V_{max} = 20, 40, 60, and 85 V were applied to the same SWNT array in air at room temperature, with a floating gate to avoid gate dielectric breakdown. Figure 1a shows SEM images of an identical SWNT after voltage ramps, which clearly show that the gap was extended only in the anode direction (one-way gap extension). The initial and final gap sizes were 63 and 337 nm, respectively. Atomic force microscopy (AFM) was also used to observe the etched SWNTs. Figures 1b-d show SEM images of SWNT gaps before and after gap extension up to V_{max} = 40 V, and an AFM image of the extended gaps in the region outlined in the SEM image. The AFM image also shows that the SWNTs on the anode side were etched from the initial gap location denoted by arrows. Some residues thinner than the SWNTs remained on the substrate, as cross section profiles from two SWNTs are shown in Figure 1e.

Similar experiments in air were performed for SWNT arrays with channel lengths of L_{ch} = 6.2 and 8.3 µm, by changing the maximum voltage from V_{max} = 40 to 100 V with 20 V steps. Typically ten SWNTs were first broken down for the following gap extension experiment under each condition, while most s-SWNTs were preserved by gate control. Each maximum voltage was applied to different SWNT arrays for the same length of time, although the size of gaps extended with a constant voltage applied for 1 s did not further change even after 1000 s in a control experiment. The sizes of the extended SWNT gaps with L_{ch} = 6.2 and 8.3 µm are plotted as a function of V_{max} in Figure 2. Error bars indicate the standard deviation of the extended gap size. Similar gap sizes and voltage-dependence were obtained for SWNT arrays of both lengths. The etching of SWNTs on anode side is self-terminated in a very short time, as is clear from time-independence of gap size. Therefore the etching length is simply determined by voltage, rather than by the product of etching rate and etching time (see Figure 2a in supplementary information (SI)). We will later discuss in detail

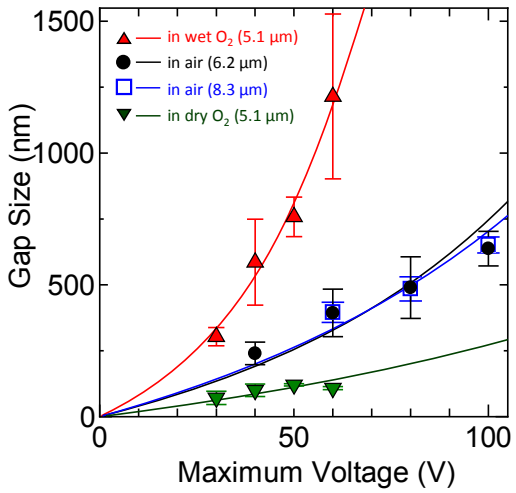

Figure 2 Gap size as a function of maximum applied voltages under various gas conditions (in air, dry O_2, and wet O_2). Circles (black) and open rectangles (blue) indicate the size of SWNT gaps extended in air with L_{ch} = 6.2 and 8.3 µm, respectively. Inversed triangles (green) represent the size of the gaps formed by electrical breakdown in dry oxygen. Red triangles corerspond to identical gap arrays further extended in wet oxygen with the same maximum voltages. L_{ch} = 5.1 µm. Solid lines represent the best-fit of the data for each condition with Equation (3).

how and why the gap size is dependent on the applied voltage. Note that exceptionally large gaps were excluded from Figure 2 because some SWNTs can be etched due to the presence of closely-placed SWNTs, as discussed later with respect to Figure 4.

We propose a mechanism for the SWNT gap size obtained by electrical breakdown on substrates as follows. The gaps initially have a gap size of <10 nm immediately after breakdown, as such small gaps were obtained in a previous study,[15] and are these gaps are readily extended by continuous application of a voltage. Chain-reaction burning of SWNTs could be considered to result in large gap formation, as reported in our previous study on organic film-assisted burning of SWNTs[4]. However, the oxygen-induced chain reaction is not expected as long as the SWNTs are directly exposed to dry air and are in contact with the substrates. This is because the collision frequency of oxygen molecules with SWNTs in air (ca. 10^9 s^{-1}) is relatively small compared to the thermal relaxation time of SWNTs on substrates (<100 ps).[21] If chain-reaction burning dominates the gap formation process, then heating of the substrates during electrical breakdown should lead to larger gap formation. However, the experimental results given in Figure S1 indicate the opposite. Furthermore, the electrical breakdown of SWNTs on substrates did not indicate a clear dependence on oxygen partial pressure (Figure S4 in SI).

The dependence of gap size on the applied voltage can explain the previous finding that electrical breakdown of longer SWNTs resulted in larger gap formation.[11,15] We simply approximate that the extended gap size is proportional to the maximum voltage for small gaps ($L_{gap} = k_1 V_{max}$, where k_1 is a constant). The breakdown voltage, the voltage required to heat up the SWNTs to oxidation temperature (typically ca. 600 °C), is proportional to the SWNT length ($V_{BD} = k_2 L_{ch}$, where k_2 was determined as 4.48 V μm^{-1} in the previous studies) for long SWNTs (L_{ch} > 1 μm).[22,23] If the voltage is ramped until an SWNT is broken, then the extended gap size will also be proportional to the SWNT length ($L_{gap} = k_1 V_{BD} = k_1 k_2 L_{ch}$). Therefore, the use of shorter SWNTs (small L_{ch}) is preferable for smaller nanogap applications in energy-efficient and highly-integrated devices.

Effect of ambient water vapor on gap extension

The dependence of gap extension on the ambient gas conditions was examined. Figure 2 (green inverted triangles) shows the size of gaps formed in SWNTs with L_{ch} = 5.1 μm by electrical breakdown up to four different V_{max} in dry oxygen gas flow. The gap size here also represents the extended gap size due to voltage application after cutting of the SWNTs, although gap formation and gap extension processes were not separated. The gaps formed in dry oxygen were smaller than those in ambient air (Figure 2), which suggests that oxygen molecules are not critical for the SWNT gap extension phenomenon, and that some other gas(es) in air play a key role.

With a focus on the water vapor in air, the gaps were further extended in wet oxygen with the same maximum voltages as those in dry oxygen. Figure 2 (red triangles) shows that the extended gap size achieved in wet oxygen is much larger than that under other conditions with lower relative humidity (RH) (wet oxygen ca. 100%RH, dry oxygen ca. 0%RH, and laboratory ambient air 30-60%RH). Gap extension experiments conducted in wet nitrogen (data not shown) revealed similar results to those in wet oxygen, which also excludes the importance of oxygen in the gap extension process. Higher humidity resulted in larger gap sizes, which indicates that water vapor plays a key role in the voltage-driven extension of SWNT gaps. Based on this knowledge, the smaller gap formation by breakdown in Ar gas flow (L_{gap} = 30-100 nm) than in air (L_{gap} = 30-200 nm), as reported previously,[11] can be explained by the low humidity in the Ar gas flow, rather than by low oxygen partial pressure. Therefore, to further decrease the SWNT gap size, electrical breakdown should be performed in high-pressure dry oxygen. This is not only because dry gas prevents gap extension, but also because high-pressure oxygen lowers the breakdown voltage of SWNTs (see Figure S4 in SI).

Field emission at SWNT nanogaps

The SWNT gap extension process involves charge transfer and an etching reaction; therefore, the current-voltage (*I*-*V*) characteristics during gap extension in air were carefully observed (see Figure S3 in SI). Although no conductive materials should be left at the gaps after breakdown of all SWNTs, a small and unstable current was still observed through the SWNT gaps. Recently, field emission (Fowler-Nordheim tunneling) at SWNT gaps on substrates with L_{gap} = 23–125 nm were examined using an electrostatic force microscopy technique.[24] For gaps of m-SWNTs with any gap size or s-SWNTs with L_{gap} > 60 nm, field emission was revealed to be the dominant charge transfer mechanism. Field emission during electrical breakdown has been briefly discussed in the literature; however, there has been no detailed investigation.[25]

To elucidate the charge transfer mechanism at the SWNT gaps in the present work, field emission properties at m-SWNT nanogaps were measured in a vacuum (ca. 0.02 Pa) to avoid damage to the anode SWNTs (gap extension). An experimental device was fabricated that contains a single SWNT, as shown in Figures 3a and b. *I*-*V* characteristics were measured for SWNT gaps with L_{gap} of ca. 80 and 300 nm (L_{ch} = 8.2 and 14.1 μm, respectively), by ramping the bias voltage from 0 V, while the gate voltage was kept equal to the cathode voltage. Figure 3c shows *I*-*V* characteristics for these gaps, where steep current increases in the sub-nanoampere range were observed at 35 V (line (a) in Fig. 3c) and 110 V (line (b) in Fig. 3c). Fowler-Nordheim (FN) plots for the measurement (Figure 3d) yield almost straight lines (solid lines show the best-fits). When we assume the electrons were emitted into vacuum from SWNTs with work function of 4.8 eV,[26] the field enhancement factors γ for the gaps shown in Figures 3a and b are calculated from the slopes[27] to be 460 and 273, respectively. Note that $\gamma = F/E$, where F and E are a local field at the emitter surface and the macroscopic field (applied voltage V divided by the inter-electrode distance L_{ch}), respectively. Despite the large difference in sample configuration, the field enhancement

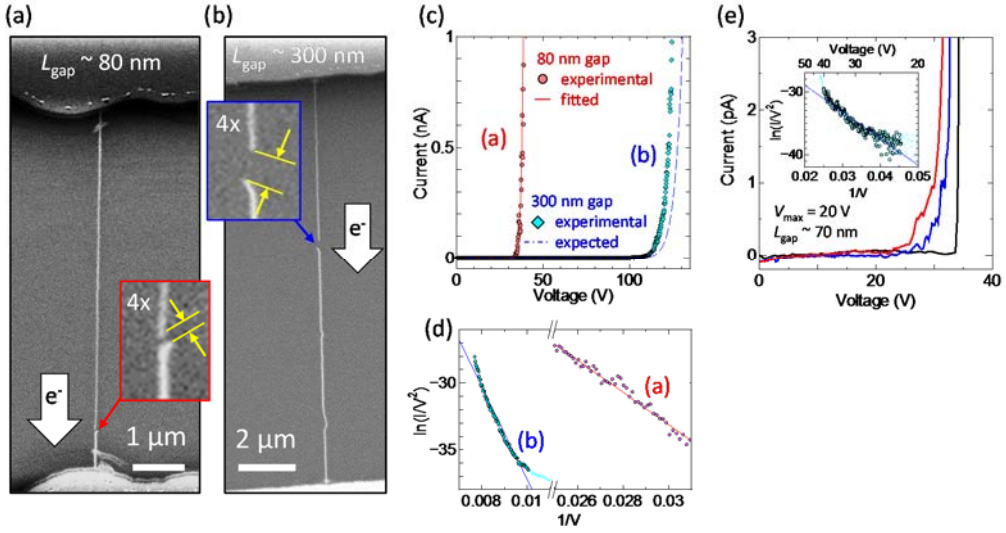

Figure 3 (a,b) SEM images of single SWNT gaps with L_{gap} = 80 and 300 nm, respectively. Insets show enlarged images of the gaps. (c) *I-V* characteristics in vacuum and (d) FN plots of the SWNT gaps shown in (a,b). Red solid and blue dashed lines represent the fitted field emission properties with the data for the 80 nm gap and the expected field emission properties of geometrical features of the 300 nm gap, respectively. (e) *I-V* characteristics of three SWNT gaps formed with voltage application up to V_{max} = 20 V. Inset: The current at 20 V (= V_{max}) is estimated by extrapolation of the FN plot.

factors roughly correspond to a previous report for free-standing SWNT field emitters (γ = 515).[27]

The field emission characteristics for three similar SWNT gaps were also compared. Following gap formation by electrical breakdown on heated substrates (ca. 100 °C), the gaps were extended with V_{max} = 20 V in air at room temperature. The sizes of all the extended gaps were around 70 nm. As shown in Figure 3e, the *I-V* characteristics of these gaps in a vacuum shows onset voltages around 25-35 V, which were slightly larger than the maximum voltage (V_{max} = 20 V) for gap extension. These gaps were extended with V_{max} = 20 V; therefore, the minimum current required for in-air gap extension (threshold current) can be estimated from the emission current at V = 20 V in a vacuum. Extrapolation of the FN plot for the gap drawn in blue yielded a threshold current of 0.1-1 fA at V = 20 V (inset of Figure 3e, see also Figure S7 in SI), which was beyond the range of measurement due to noise in the present setup. It should be noted, however, that the field emission properties of SWNTs can be affected by the adsorption of oxygen and water molecules in air.[28,29] Note that the linear current component obtained from the device without SWNTs (I/V = 14.9 [fA V^{-1}]) was deducted in Figure 3e to exclude leakages that did not originate from the SWNTs.

Although the field emission current was measured in a vacuum, the surface leakage current via water adsorbed on the substrates must be considered as another conduction mechanism in the presence of water vapor. Charge transfer between SWNTs and water electrolyte (electrochemical reaction) requires an electric field with a specific strength at the interface. Therefore, a higher voltage is required to maintain the constant field strength for larger SWNT gaps, which may appear as the observed relation between the applied voltage and gap size (Figure 2). Even in that case, the field emission measurement in a vacuum is useful for quantification of the field enhancement at SWNT tips.

Threshold field for gap extension: voltage vs. gap size

Now the validity of the field emission electron as a cause of SWNT etching is evaluated. We suppose that the emission current is kept constant (threshold current, I_0) during the gap extension process because the gap size changes according to the ramp voltage. The FN law gives the relation between the emission current I [A], and the local field at the emitter surface F [V/m], as:[30]

$$I = A\frac{1.5\times10^{-6}}{\phi}F^2\exp\left(\frac{10.4}{\sqrt{\phi}}\right)\times\exp\left(-\frac{6.44\times10^{9}\phi^{\frac{3}{2}}}{F}\right), \quad (1)$$

where A [m^2] is the emission area and φ [eV] is the work function of the SWNTs. The local field F is obtained from the macroscopic field E and the field enhancement factor γ at the emitter surface. The FN law indicates that the local field F (= γE) is a constant value of F_0 during gap extension under this premise, although F_0 differs according to the ambient gas conditions. Even when we assume the water-related leakage current as the charge transfer mechanism, the local field F also dominates the electrochemical oxidation (gap extension). Previous studies have reported models to estimate the field enhancement factor γ from geometric features, such as the length of the CNT emitter h, the distance between the flat anode and CNT tips D, and the radius r, for free-standing CNT emitters.[27,31,32] When the inter-electrode distance is large compared to the CNT height, the field enhancement factor γ is simply estimated by the CNT height and the radius ($\gamma_0 \propto 1+\sqrt{h/2r}$.[32] For the case of smaller D, $\gamma = \gamma_0\times\{1+a\times[D/(D+h)]^{-1}-b\times[D/(D+h)]\}$ is often used as the modified relation,[27] where a and b are constants. The relation can be

further rewritten to match the configuration of the present samples (see Figure S5 in SI for details):

$$\gamma = c\left(1+\sqrt{\frac{L_{ch}-L_{gap}}{4r}}\right)\left(1+a\frac{L_{ch}}{L_{gap}}-b\frac{L_{gap}}{L_{ch}}\right), \quad (2)$$

where c and L_{ch} are a constant and the channel length (original SWNT length) of the device, respectively. From the relation $F = \gamma V_{max}/L_{ch}$, the maximum voltage V_{max} that gives the constant local field F_0 at the SWNT tips for any gap size L_{gap} is expressed as:

$$V_{max}(L_{gap}) = \frac{F_0 L_{ch}}{\gamma}. \quad (3)$$

Equation (3) was fitted to the experimental data in Figure 2 with a and F_0/c as fitting parameters. The diameter of all the SWNTs was assumed to be 1.5 nm.[33] When a = 0.11, the fitting lines corresponded well with the trend of the experimental data under all the conditions, as shown in Figure 2 (see Figure S6a in SI for different a values). The b constant has little effect on the fitting results; therefore, b was set at zero. Compared to the threshold field $F_{0,air}$ obtained from the data in air (L_{ch} = 6.2 μm), the other threshold field strengths for the gap extension in wet oxygen (L_{ch} = 5.1 μm), in air (L_{ch} = 8.3 μm), and in dry oxygen (L_{ch} = 5.1 μm) were $0.47F_{0,air}$, $1.04F_{0,air}$, and $1.80F_{0,air}$, respectively. Enhancement of the emission current at a given field by water adsorption on SWNTs[29,34] can account for the lower threshold field under higher humidity conditions. Switching of the major charge transfer mechanisms from field emission to surface leakage current is another possible explanation for the low threshold field in wet oxygen.

This relation was further applied to calculation of the *I-V* characteristics for field emission using the FN law (Equation (1)). Now, for simplicity, an SWNT diameter d_t of 1.5 nm and φ = 4.8 eV are supposed. The emission area A is estimated from the *y*-intercept of the FN plot to be 7.0×10^{-12} m^2. First, c = 0.66 was obtained by fitting with the field emission characteristics of the 80 nm gap shown in Figure 3c (red line). The *I-V* characteristics for the 300 nm gap were then predicted from the gap configuration using Equations (1) and (2). As shown in Figure 3c, the predicted *I-V* characteristics (blue dashed line) are in good accordance with the experimental results (see Figure S6b in SI for different a values). This indicates that the relation between the geometric features and the field enhancement factor γ (Equation (2)) is useful to predict the field emission characteristics of SWNT gaps on substrates, and also that the gap extension is dominated by the geometrically-derived field enhancement at the SWNT tips. Note that L_{ch} of 12.5 and 11.5 μm were substituted into Equation (2) for 80 and 300 nm gaps, respectively, because the length of the SWNTs on the cathode side rather than the distance between two metal (Pd) contacts influence the field enhancement (see Figure S6 in SI). The threshold field strength in air $F_{0,air} = 1.7\times10^9$ V m^{-1} was obtained from the threshold current I_0 = 0.1-1 fA. Field emission into a vacuum was assumed here, although a similar comparison of the 80 nm and 300 nm gaps is possible for field emission (FN tunneling) into SiO_2 with slight modification of the parameters.

Taking field-emission electrons and water molecules into account, we propose two mechanisms for SWNT etching as follows. In ambient air, the SWNT surface is covered with a few layers of water molecules.[35,36] The first possible mechanism is electrochemical etching of anode SWNTs,[37] where charge transfer occurs via field emission or water-mediated surface current. Electrochemical oxidation first occurs on the SWNT surfaces, which forms covalently functionalized groups. The locally functionalized SWNTs are then removed through further oxidation. The total reaction can be expressed as C(SWNT) + $3OH^- \rightarrow CO_3^{2-} + 3H^+ + 4e^-$. In contrast to the electrochemical etching of SWNTs in bulk electrolytes, physisorbed water from the air is unlikely to form an electric double layer under the conditions of the present experiments, which typically strengthens the field at the SWNT-electrolyte interfaces. Instead, field enhancement at the SWNT tips due to the ultrahigh aspect ratio may play an important role in the oxidation process. SWNT etching may continue either until the gaps are extended to a sufficient extent for the emission current to be negligible or until the local field at the tips become weak enough to not cause the electrochemical reaction.

A second possible explanation for the gap extension is as follows. Electrons emitted from cathode tips are accelerated by an electric field while flowing between the SWNT gaps. Physisorbed water molecules on the SWNT tips are ionized by accelerated electrons and turn into highly reactive species, such as OH·, H·, and HO_2· radicals. These species then etch neighboring carbon atoms of the SWNTs to form CO, CO_2, and various hydrocarbons. A similar etching phenomenon was reported in studies on CNT cutting[6] and the machining of CNT forests,[38] where CNTs were cut with a low-energy focused electron beam (with SEM) in the presence of water vapor inside the chamber.

Electrical breakdown on heated substrates resulted in smaller gap formation because water molecules on the SWNT surfaces desorb at high temperature, even under the same water vapor pressure (see Figure S1 in SI). This indicated the importance of adsorbed water molecules rather than water molecules in the gas phase, which supports both mechanisms proposed here. Even when the emission current is sufficiently large, the gaps are not extended in the absence of water molecules on anode side SWNTs (*e.g.*, in a vacuum).

Remote etching among adjacent SWNTs

We also identified the remote etching phenomenon of anode SWNTs parallel to cathode SWNTs with small inter-SWNT spacing, as shown in Figure 4a. Here, the SWNTs that connect only with metal anodes or cathodes are referred to as A-SWNTs or C-SWNTs, respectively. Gaps were first formed at a red arrow position and then extended to an L_{gap} of a few microns, whereas the other two gaps were only extended to an L_{gap} of a few hundreds nanometers. This can be explained by field enhancement between side walls of A- and C-SWNTs,[39] which induce the etching of adjacent A-SWNTs, as schematically shown in Figure 4b. Red and blue colors in the schematic illustration indicate high and low electric potential, respectively.

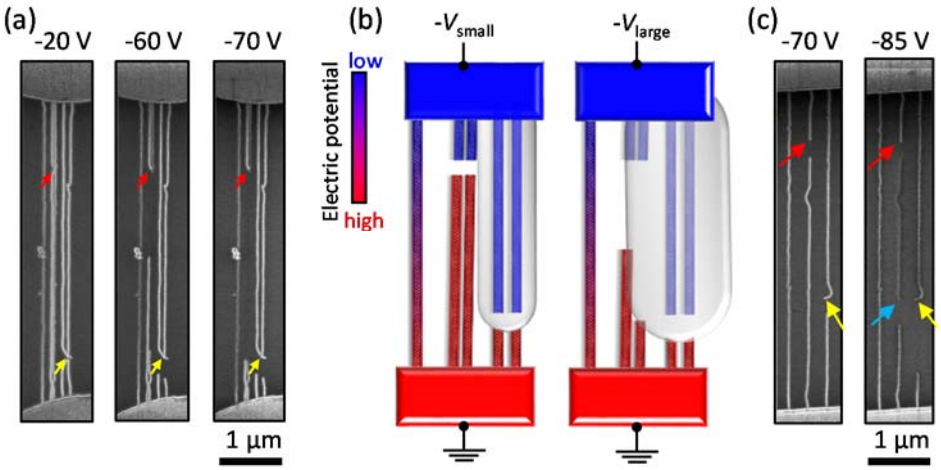

Figure 4 (a) SEM images of five parallel SWNTs. Each image was taken after voltage application up to V_{max} as indicated. The red and yellow arrows indicate the initial gap location on the anode and cathode SWNTs (A- and C-SWNTs), respectively. Two A-SWNTs in the middle were etched from over a few microns because of right C-SWNTs. (b) Schematic illustrations of the electric potential at two stages of the SWNT array in (a). Left: after the gap formation at the red arrow position, corresponding to 20 V < V_{max} < 60 V. Right: after the remote etching of A-SWNTs, corresponding to V_{max} = 60 V. Field emission from C-SWNTs can affect A-SWNTs inside the gray area. (c) SEM images for the double cutting of a single SWNT. Secondary cutting of the middle SWNT occurred at the position marked by blue arrow.

A-SWNTs (red) within a certain distance from C-SWNTs (inside the gray region) are etched away. Although this etching mechanism is intrinsically the same as gap extension, the extent to which the SWNTs are etched away is determined by the distance between the two gaps of A- and C-SWNTs. In addition, for etching to occur is dependent on the inter-SWNT spacing of two parallel SWNTs and the applied voltage. If uniformly dense SWNT arrays can be grown and also m- and s-SWNTs are intentionally cut near cathodes and anodes, respectively, then this parallel etching could be used to eliminate only m-SWNTs by utilizing selective field emission from the side wall of s-SWNTs (see Figure S8 in SI for details of the possible process).

This type of etching may deteriorate the removal selectivity during electrical breakdown by cutting or damaging the adjacent s-SWNTs. For example, the SWNT that did not bridge two metallic contacts due to electrical breakdown was cut again around the neighboring nanogap, as indicated by a blue arrow in Figure 4c (also see Figure S3). This indicates that SWNTs can be broken down without Joule self-heating if nanogaps are present in the vicinity. The SWNT segment between the red and blue arrows had a low contrast to the substrate in the SEM image, which also indicates the physical isolation of the SWNT segment from other SWNTs and metal electrodes.[40]

If ionization of water by accelerated electrons induces the cutting of unbridged SWNTs, then operation with voltages smaller than the ionization energy of water (ca. 12.7 eV) would be helpful to avoid deterioration of the removal selectivity. The electrical breakdown of SWNT arrays (ca. 20 SWNTs μm^{-1}, L_{ch} = 2 μm), where a bias voltage of up to 20 V was applied, resulted in the correlated breakdown of neighboring SWNTs,[19] though this was previously explained in a different way.[20] In contrast, the electrical breakdown of higher-density but shorter SWNT arrays (>100 SWNTs μm^{-1}, L_{ch} = 400 nm), where the breakdown voltage is always <8 V, successfully cut only m-SWNTs (current retention >20%).[41] Note that a relatively thick gate dielectric (Al_2O_x, 25 nm equivalent oxide thickness) compared to the inter-SWNT spacing (<10 nm) was used, and high electric field (>10 V μm^{-1}) was applied.[41] The results of adjacent SWNT etching will thus provide a guide to the design of appropriate device structures and the experimental conditions required for successful SWNT purification.

Conclusions

We have reported on the field emission and voltage-driven gap extension phenomena for SWNTs on substrates. The gap extension clearly showed one-directionality and dependence on the applied voltage and humidity. Therefore, the SWNT gap size can be controlled by changing the water vapor pressure, substrate temperature, and voltage. Size controllability will broaden the application of nanogaps, especially as nanoscale electrodes. The *I-V* characteristics of single gap devices in vacuum indicated FN tunneling features, which corresponds well with the characteristics predicted from the FN law and the field enhancement model that was calibrated using the gap extension results. Electrochemical oxidation and charge transfer via field emission are thus possible driving forces of SWNT gap extension. In addition, unintentional damage to the neighboring SWNTs induced by field enhancement between adjacent SWNTs should be minimalized when electrical breakdown is employed to selectively cut m-SWNTs for semiconductor applications.

Experimental

SWNT growth and device fabrication: Metal electrodes (Ti/Pd or Ti/Au; 5/20 nm) were photolithographically patterned using sputtering on a highly p-doped Si substrate with a 100 nm thick thermal oxide layer. Horizontally aligned SWNTs were grown by the alcohol catalytic chemical vapor deposition method[33,42] on

r-cut crystal quartz substrates, and then transferred onto the Si/SiO_2 substrates with patterned electrodes via poly(methyl methacrylate) (PMMA) thin films.[43] Unwanted SWNTs outside channel regions were etched by oxygen plasma to isolate the devices. Each device has 20 µm wide electrodes with 5-15 µm spacing and typically contains 30 SWNTs (density of 1.5 SWNTs μm^{-1}), which is suitable to avoid interaction and bundling among adjacent SWNTs.

SWNT nanogap preparation: SWNT nanogaps were prepared using the electrical breakdown technique. Electrical breakdown was first performed on a hotplate (ca. 100 °C) because the breakdown of SWNTs on heated substrates was found to result in smaller gap formation than that at room temperature, as shown in Figure S1 of the SI. The gap location was checked by scanning electron microscopy (SEM; 1 kV, S-4800, Hitachi Co., Ltd.) or atomic force microscopy (AFM; SPI3800N, SII).

Nanogap extension: A ramp voltage was applied from 0 to negative maximum voltage ($-V_{max}$) to the nanogaps for a typical period of 100 s at room temperature, and the extent of gap extension was observed. The gap extension experiments were conducted under various gas conditions, such as in air, and in dry or wet oxygen gas flow. Dry oxygen was obtained directly from an oxygen gas cylinder and was flowed onto the substrates. Wet oxygen was obtained using the water bubbler technique (see the setup used in Figure S2b of the SI) at room temperature to provide saturated water vapor (ca. 3 kPa). A voltage was also applied to SWNT gaps in vacuum (ca. 0.02 Pa) to avoid gap extension and observe the *I-V* characteristics at gaps of a certain size.

Acknowledgements

Part of this work was financially supported by Grants-in-Aid for Scientific Research (Nos. 15H05760, 25107002, 26420135) and the IRENA Project of JST-EC DG RTD, Strategic International Collaborative Research Program (SICORP). This work was partly conducted at the Center for Nano Lithography & Analysis, and VLSI Design and Education Center (VDEC), the University of Tokyo. K.O. was financially supported by a Japan Society for the Promotion of Science (JSPS) Fellowship (15J07857).

References

1 P. G. Collins, M. S. Arnold and P. Avouris, *Science*, 2001, **292**, 706–709.
2 N. Patil, A. Lin, J. Zhang, H. Wei, K. Anderson, H.-S. P. Wong and S. Mitra, *IEEE Trans. Nanotechnol.*, 2011, **10**, 744–750.
3 M. M. Shulaker, G. Hills, J. Payne, H. Wei, H.-Y. Chen, H.-S. P. Wong and S. Mitra, *Nature*, 2013, **501**, 526–30.
4 K. Otsuka, T. Inoue, S. Chiashi and S. Maruyama, *Nanoscale*, 2014, **6**, 8831–8835.
5 J. Li, A. D. Franklin and J. Liu, *Nano Lett.*, 2015, **15**, 6058–6065.
6 T. D. Yuzvinsky, A. M. Fennimore, W. Mickelson, C. Esquivias and A. Zettl, *Appl. Phys. Lett.*, 2005, **86**, 053109.
7 C. Thiele, M. Engel, F. Hennrich, M. M. Kappes, K.-P. Johnsen, C. G. Frase, H. V. Löhneysen and R. Krupke, *Appl. Phys. Lett.*, 2011, **99**, 173105.
8 A. Cui, H. Dong and W. Hu, *Small*, 2015, **11**, 6115–6141.
9 X. Guo, J. P. Small, J. E. Klare, Y. Wang, M. S. Purewal, I. W. Tam, B. H. Hong, R. Caldwell, L. Huang, S. O'brien, J. Yan, R. Breslow, S. J. Wind, J. Hone, P. Kim and C. Nuckolls, *Science*, 2006, **311**, 356–9.
10 C. W. Marquardt, S. Grunder, A. Błaszczyk, S. Dehm, F. Hennrich, H. V Löhneysen, M. Mayor and R. Krupke, *Nat. Nanotechnol.*, 2010, **5**, 863–867.
11 F. Xiong, A. D. Liao, D. Estrada and E. Pop, *Science*, 2011, **332**, 568–70.
12 P. Collins, M. C. Hersam, M. Arnold, R. Martel and P. Avouris, *Phys. Rev. Lett.*, 2001, **86**, 3128–3131.
13 A. D. Liao, R. Alizadegan, Z.-Y. Ong, S. Dutta, F. Xiong, K. J. Hsia and E. Pop, *Phys. Rev. B*, 2010, **82**, 205406.
14 E. Pop, D. A. Mann, Q. Wang, K. E. Goodson and H. Dai, *Nano Lett.*, 2006, **6**, 96–100.
15 P. Qi, A. Javey, M. Rolandi, Q. Wang, E. Yenilmez and H. Dai, *J. Am. Chem. Soc.*, 2004, **126**, 11774–5.
16 J. Y. Huang, S. Chen, S. H. Jo, Z. Wang, D. X. Han, G. Chen, M. S. Dresselhaus and Z. F. Ren, *Phys. Rev. Lett.*, 2005, **94**, 236802.
17 K. Mølhave, S. B. Gudnason, A. T. Pedersen, C. H. Clausen, A. Horsewell and P. Bøggild, *Nano Lett.*, 2006, **6**, 1663–1668.
18 T. Kim, T. J. Kang, K. Li, E. Y. Jang, J. S. Lee, D. K. Seo, H. Im and Y. H. Kim, *Sensors Actuators B Chem.*, 2012, **173**, 517–522.
19 S. Shekhar, M. Erementchouk, M. N. Leuenberger and S. I. Khondaker, *Appl. Phys. Lett.*, 2011, **98**, 243121.
20 M. A. Wahab and M. A. Alam, *IEEE Trans. Electron Devices*, 2014, **61**, 4273–4281.
21 Z.-Y. Ong and E. Pop, *Phys. Rev. B*, 2010, **81**, 155408.
22 E. Pop, *Nanotechnology*, 2008, **19**, 295202.
23 E. Pop, D. A. Mann, K. E. Goodson and H. Dai, *J. Appl. Phys.*, 2007, **101**, 093710.
24 K. A. S. Araujo, A. P. M. Barboza, T. F. D. Fernandes, N. Shadmi, E. Joselevich, M. S. C. Mazzoni and B. R. A. Neves, *Nanoscale*, 2015, **7**, 16175–16181.
25 A. Javey, J. Guo, M. Paulsson, Q. Wang, D. Mann, M. Lundstrom and H. Dai, *Phys. Rev. Lett.*, 2004, **92**, 106804.
26 S. Suzuki, C. Bower, Y. Watanabe and O. Zhou, *Appl. Phys. Lett.*, 2000, **76**, 4007.
27 J.-M. Bonard, K. Dean, B. Coll and C. Klinke, *Phys. Rev. Lett.*, 2002, **89**, 197602.
28 A. Wadhawan, R. E. Stallcup, K. F. Stephens, J. M. Perez and I. A. Akwani, *Appl. Phys. Lett.*, 2001, **79**, 1867.
29 K. A. Dean, P. von Allmen and B. R. Chalamala, *J. Vac. Sci. Technol. B Microelectron. Nanom. Struct.*, 1999, **17**, 1959.
30 I. Brodie and C. A. Spindt, in *Advances in Electronics and Electron Physics*, 1992, vol. 7, pp. 1–106.
31 C. J. Edgcombe and U. Valdrè, *J. Microsc.*, 2001, **203**, 188–194.
32 R. C. Smith, D. C. Cox and S. R. P. Silva, *Appl. Phys. Lett.*, 2005, **87**, 103112.
33 T. Inoue, D. Hasegawa, S. Badar, S. Aikawa, S. Chiashi and S. Maruyama, *J. Phys. Chem. C*, 2013, **117**, 11804–11810.
34 A. Maiti, J. Andzelm, N. Tanpipat and P. von Allmen, *Phys. Rev. Lett.*, 2001, **87**, 155502.
35 Y. Homma, S. Chiashi, T. Yamamoto, K. Kono, D. Matsumoto, J. Shitaba and S. Sato, *Phys. Rev. Lett.*, 2013, **110**, 157402.

36 S. Chiashi, K. Kono, D. Matsumoto, J. Shitaba, N. Homma, A. Beniya, T. Yamamoto and Y. Homma, *Phys. Rev. B*, 2015, **91**, 1–5.
37 D. Wei, Y. Liu, L. Cao, H. Zhang, L. Huang, G. Yu, H. Kajiura and Y. Li, *Adv. Funct. Mater.*, 2009, **19**, 3618–3624.
38 B. Rajabifar, S. Kim, K. Slinker, G. J. Ehlert, A. J. Hart and M. R. Maschmann, *Appl. Phys. Lett.*, 2015, **107**, 143102.
39 Y. Shiratori, K. Furuichi, S. Noda, H. Sugime, Y. Tsuji, Z. Zhang, S. Maruyama and Y. Yamaguchi, *Jpn. J. Appl. Phys.*, 2008, **47**, 4780–4787.
40 R. Y. Zhang, Y. Wei, L. A. Nagahara, I. Amlani and R. K. Tsui, *Nanotechnology*, 2006, **17**, 272–276.
41 M. M. Shulaker, G. Pitner, G. Hills, M. Giachino, H.-S. P. Wong and S. Mitra, in *2014 IEEE International Electron Devices Meeting*, 2014, vol. 4, pp. 33.6.1–33.6.4.
42 S. Maruyama, R. Kojima, Y. Miyauchi, S. Chiashi and M. Kohno, *Chem. Phys. Lett.*, 2002, **360**, 229.
43 L. Jiao, B. Fan, X. Xian, Z. Wu, J. Zhang and Z. Liu, *J. Am. Chem. Soc.*, 2008, **130**, 12612–3.

Supplementary Information

Field emission and anode etching during formation of length-controlled nanogaps in electrical breakdown of horizontally aligned single-walled carbon nanotubes

*Keigo Otsuka,[a] Taiki Inoue,[*a] Yuki Shimomura,[a] Shohei Chiashi[a] and Shigeo Maruyama[*a,b]*

[a] Department of Mechanical Engineering, The University of Tokyo, 7-3-1 Hongo, Bunkyo-ku, Tokyo 113-8656, Japan

E-mail: inoue@photon.t.u-tokyo.ac.jp, maruyama@photon.t.u-tokyo.ac.jp

[b] Energy NanoEngineering Lab., National Institute of Advanced Industrial Science and Technology (AIST), 1-2-1 Namiki, Tsukuba, Ibaraki. 305-8564, Japan

1. Effect of substrate heating during electrical breakdown on gap size

If the gap size formed by electrical breakdown is dominated by oxygen-induced chain reaction, substrate heating during voltage application will simply increase the gap size. Figure S1 shows the histograms of gap size at three different substrate temperatures (~20, ~60, ~100 ˚C). Contrary to the expectation, the gap size drastically decreased with increasing substrate temperature. This indicates the gap size formed by in-air electrical breakdown is not determined by chain-reaction burning. Note that slightly different maximum voltage was applied for three SWNT arrays (~60, 43, 45 V for ~20, 60, 100 ˚C, respectively). Wide distribution for lower temperature experiments may be attributed to the etching due to field enhancement between adjacent SWNTs (Figure 4) because electrical breakdown of long SWNTs (~15 μm) requires high voltage application (~60 V).

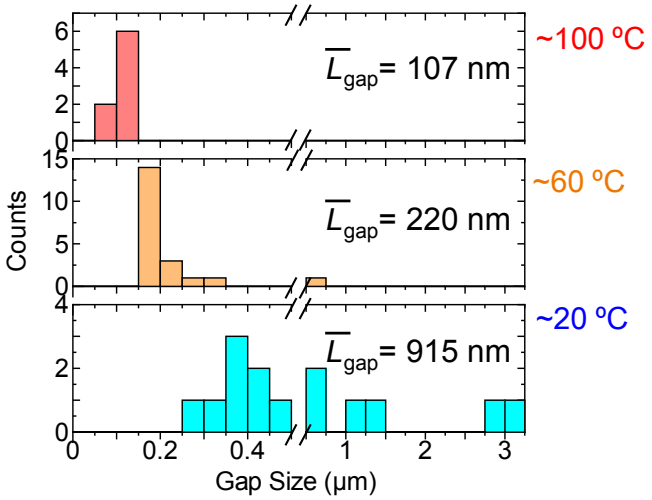

Figure S1. Distribution of gap size obtained by electrical breakdown in air at different temperatures.

2. Experimental details

We show the schematic illustration of time evolution of both voltage and gap size during gap extension experiment in Figure S2a. Voltage was increased from zero to a certain value (V_{max}: 30-100 V) typically in 100 s. Since this anode etching phenomena is self-limited due to the decreased field

enhancement associated with gap extension, the gap size seems to change with voltage. If we take a closer look at the change in voltage, it shows stepwise increase (by 30-100 mV) rather than continuous increase because of machine constraint as shown in the inset. We guess the gap size are readily increased just after each stepwise increase of voltage and keeps constant until next voltage increment. The current I and the local field at the SWNT tips F must be slightly larger than threshold (I_0, F_0) during gap growth, and then go down to threshold for a while.

To control humidity of ambient gas, pure oxygen gas or oxygen through a water bubbler was sprayed on the sample during electrical breakdown and gap extension processes. Figure S2b shows the schematic illustration of the gap extension in wet oxygen (oxygen saturated with water vapor at room temperature). Almost no water droplets were observed on the substrates by optical microscope during the wet oxygen spraying, which indicates the relative humidity of ~100%.

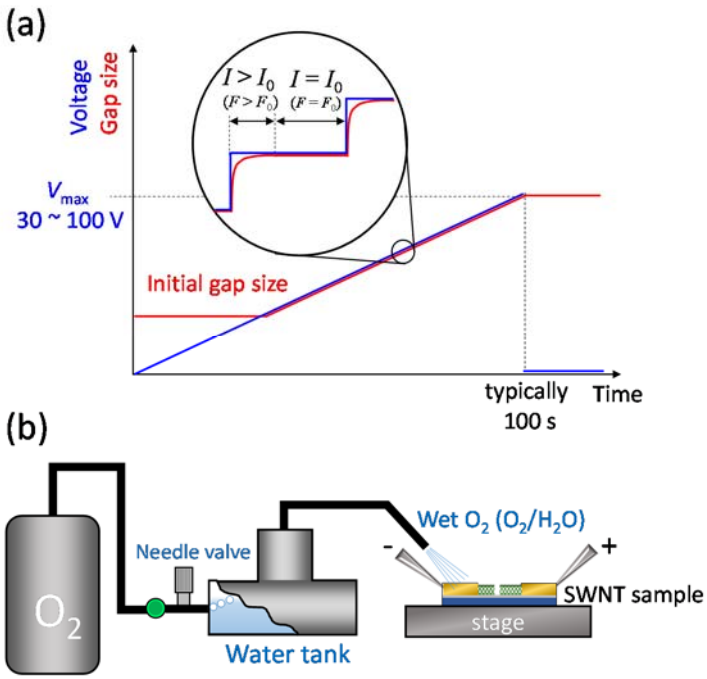

Figure S2. (a) Schematic illustration of time evolution of voltage and gap size. Inset shows the gap size change which follows the stepwise increase of voltage. (b) Schematic illustration of the gap extension in wet oxygen. Oxygen gas through a water bubbler (kept at room temperature) was directly sprayed onto the samples during the voltage application to SWNT gaps.

3. Gap extension of SWNT arrays and current transition

Throughout the study, the gaps in SWNT arrays were extended as shown in Figure S3. Red arrows indicate the gaps created by electrical breakdown process on hotplates. After further voltage application process, new gaps were formed, but not included in the calculation of the extended gap size. Some SWNTs have two gaps as second gaps are indicated by yellow arrows, probably due to the influence of adjacent gaps. Taking a closer look at the current transition during the gap extension (inset), small (~nA) and unstable current was observed after all the SWNTs were broken down ($V >$ 76 V). This current suggests the conduction through SWNT gaps which induces the gap extension.

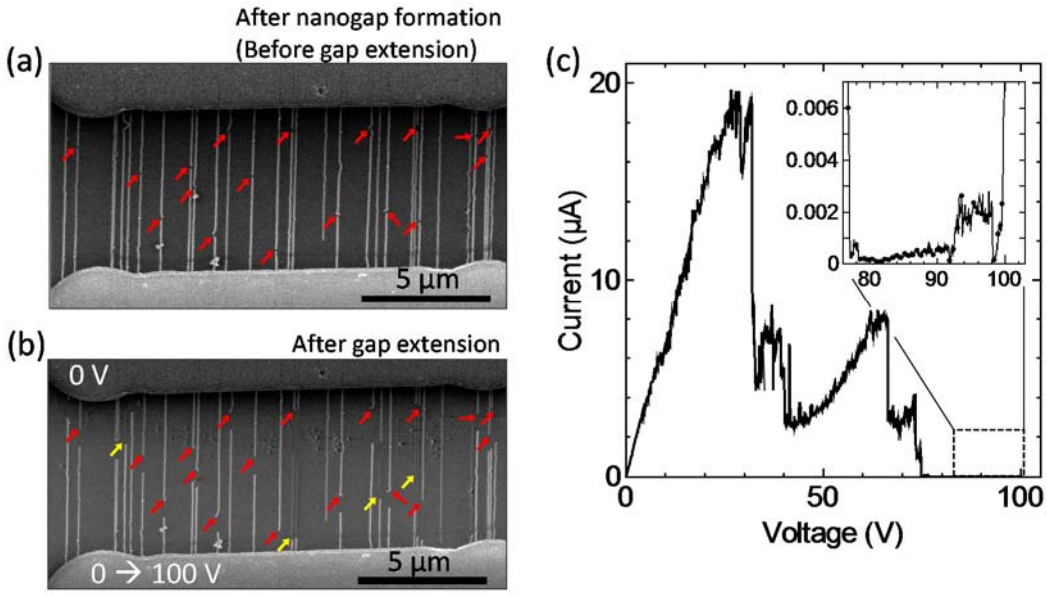

Figure S3. (a) SEM image of SWNT arrays after nanogap formation by electrical breakdown on hotplates (~100 ºC), and (b) after gap extension under ambient condition. Yellow arrows indicate the cutting of already-broken SWNTs caused by adjacent gaps. (c) Current transition during the gap extension. Inset shows enlarged graph with voltage larger than 76 V, where all the SWNTs were broken.

4. Effect of oxygen pressure during electrical breakdown on gap size

It is well known that electrical breakdown of SWNTs is affected by oxygen partial pressure.[1] With a focus on chemical reaction which induces the breakdown, higher oxygen pressure (p_{O2}) seems to lead to higher reaction rate even at the same temperature. Thus, the breakdown temperature and the breakdown power (power input needed to induce SWNT breakdown) should be high/large at low oxygen pressure.

Vacuum chamber was used to control the pressure. After evacuating the chamber (< 10 Pa) with a rotary pump, oxygen was introduced. Figure S4a shows current transition (black lines) during electrical breakdown process and the breakdown power density per unit length (blue circles). The breakdown power P_{BD} [W] was obtained by multiplying current drop ΔI [A] and applied voltage V [V] ($P_{BD} = \Delta I \times V$). The breakdown voltage and the breakdown power density were much higher at p_{O2} < 0.1 kPa than those at p_{O2} ~ 95 kPa. However, the gap size does not have clear dependence on oxygen pressure (Figure S4b). This suggest that breakdown (cutting) and gap formation of SWNTs are based on different mechanisms. Note that different V_{max} was applied for the experiments under different oxygen pressure, and the gap size was slightly dependent on V_{max} (Figure S4b inset) as described in the main article.

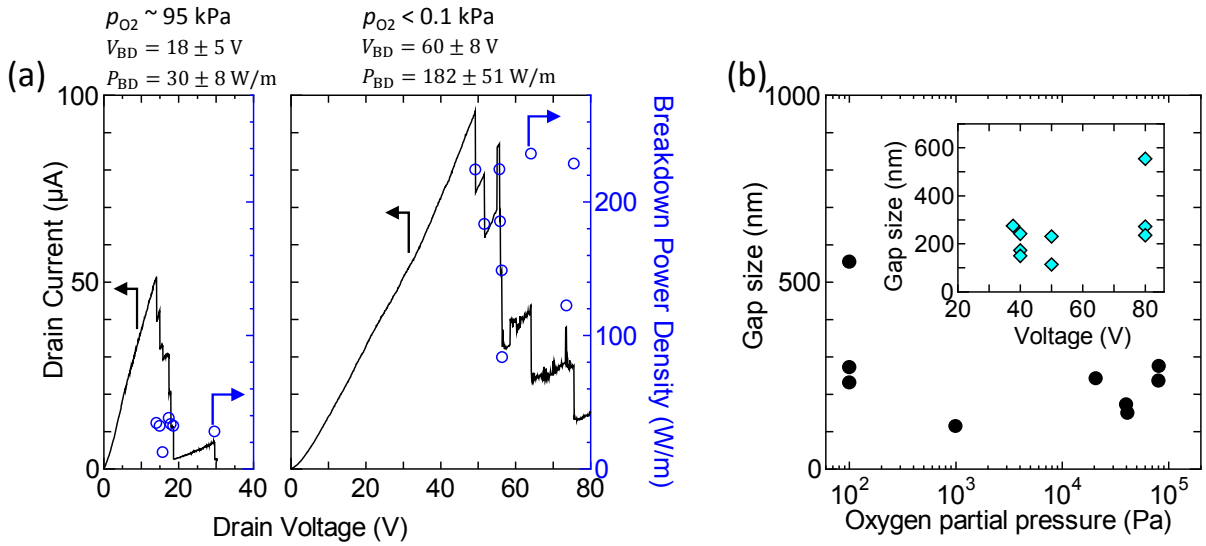

Figure S4. SWNT gaps were formed by electrical breakdown at various oxygen partial pressures (p_{O2}). (a) Current transition (black) and breakdown power density (P_{BD} [W/m], blue circle) during the electrical breakdown. (b) Oxygen pressure vs Gap size. Each data point shows the average size of typically ~10 SWNT gaps. Channel length L_{ch} = 5 μm. Inset: Gap size as a function of V_{max} shows dependence on applied voltage despite the electrical breakdown under various oxygen pressures.

5. Assumed sample configuration for field enhancement modeling

The relation between geometrical features of SWNT gaps (L_{gap} and L_{ch}) and field enhancement factor γ was obtained by fitting the experimental data shown in Figure 2. When the distance between emitter tips and anode D is large ($D > 3h$), a field enhancement factor γ_0 of the emitter shown in Figure S5a is purely a factor of the CNT height and radius and written as[2]

$$\gamma_0 \propto 1 + \sqrt{\frac{h}{2r}} \,. \qquad (1)$$

However, when D (or gap size) is small compared to SWNT length h, equation (2) will be corrected as[34]

$$\gamma = \gamma_0 \left[1 + a\left(\frac{D}{D+h}\right)^{-1} - b\left(\frac{D}{D+h}\right)\right] \quad (2)$$

Since the configuration of our sample is different from conventional field emitters, we assumed the gaps are located in the middle of channels for simplicity so that the same relation as tip-plane configuration can be used (Figure S5b). This assumption is useful also because the position of the gaps is randomly scattered around the middle of the channel.[1] Using geometrical parameters of our samples, equation (2) can be further rewritten as follows.

$$\gamma = c(1 + \sqrt{\frac{L_{\mathrm{ch}} - L_{\mathrm{gap}}}{4r}})(1 + a\frac{L_{\mathrm{ch}}}{L_{\mathrm{gap}}} - b\frac{L_{\mathrm{gap}}}{L_{\mathrm{ch}}}) \quad (3)$$

Here, three unknown parameters, *a*, *b*, and *c*, appear in the equation. The SWNTs of our samples lay on substrates as shown in Figure S5c, but we did not consider the difference between Figure S5b and c for simplicity. Since usually $L_{\mathrm{gap}} << L_{\mathrm{ch}}$ in our experiments, *b* has little effect and thus set to zero. Then proper value of $a = 0.11$ was obtained from V_{max} vs L_{gap} (Figure 2). Fitting lines when *a* is different ($a = 0.01$, 0.5) are shown in Figure S6a. Finally, *c* (= 0.66) was obtained from the field emission properties of the 80-nm-gap in vacuum and the FN law (Figure 3c). Also, *I*-*V* characteristics for the 300-nm-gap estimated from the FN law and geometrical features are shown in Figure S6b. As shown in Figure S6c, L_{ch} obtained by doubling the length of SWNT segments on cathode side $L_{\mathrm{C\text{-}SWNT}}$ (strictly speaking, $L_{\mathrm{ch}} = 2L_{\mathrm{C\text{-}SWNT}} + L_{\mathrm{gap}}$) was used to calculate field enhancement factors, which was different from the cathode-anode distance (Figure S6c). It is because we know the exact value of $L_{\mathrm{C\text{-}SWNT}}$ from SEM observation, and $L_{\mathrm{C\text{-}SWNT}}$ is more important when the field enhancement at SWNT tips on cathode side is considered. If *a* is large (for example $a = 0.5$), field enhancement factor γ is inversely proportional to gap size L_{gap}. At that case, gap size will be proportional to applied voltage.

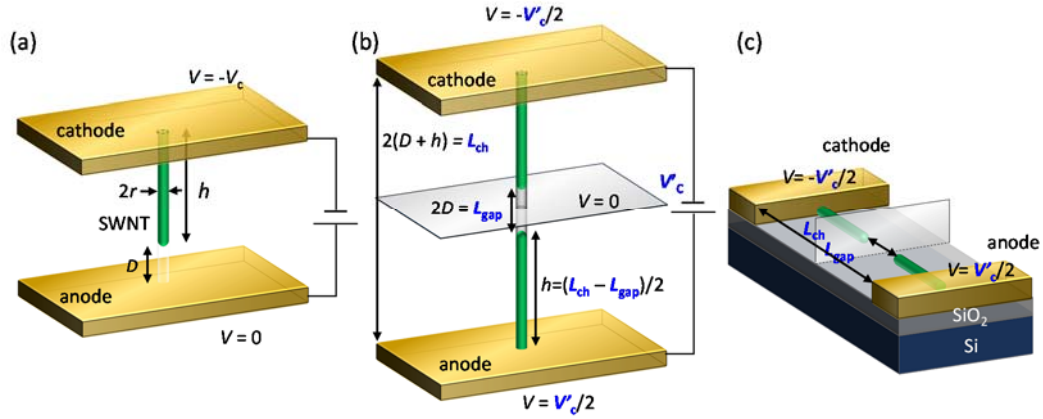

Figure S5. Schematic illustrations of sample configuration used for field enhancement modeling. (a) Typical configuration with SWNT tip-to-flat metal electrode. (b) Tip-to-tip configuration (free standing) assuming the gap is located at the center. (c) SWNT gap on substrates (our samples).

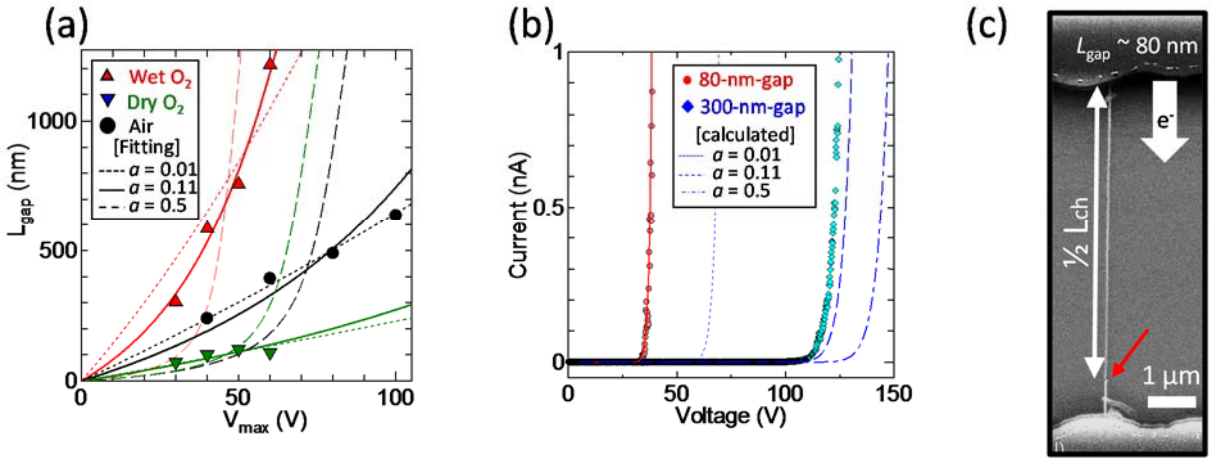

Figure S6. (a) Fitting lines of the data shown in Figure 2 with the equation [$V_{max}(L_{gap}) = F_0 L_{ch}/2\gamma$], which give the constant local field F_0 for variable gap size. a and F_0/c are fitting parameters. (b) Predicted field emission current for the 300-nm-gap. Dotted lines, dashed lines, and dash-dotted lines are obtained when a = 0.01, 0.11, 0.5 in equation (2), respectively. (c) SEM image of the 80-nm-gap. The gap was not located in the middle.

6. Extrapolation of threshold current for gap extension

The current needed for the gap extension is too small to detect. When ramp voltage was applied to a single gap in air, usually no current was detected. We estimated the minimum current (threshold

current) needed to extend the SWNT gaps in air by extrapolating the FN plots obtained in vacuum. Field emission current can be simply expressed by two constants and voltage as $I = C_1V^2\exp(-C_2/V)$. Figure S7a and b show the fitting in an *I-V* curve and an FN plot, respectively. The fitting and extrapolation of the gap in Figure 3e (red) yields threshold current (at V = 20 V) of 0.56-1.70 fA. Also, the gap in Figure 3e (blue) gives similar threshold current of 0.33 fA (Figure S7c). We should note that this estimation is appropriate unless C_1 and C_2 are affected by water, oxygen, nitrogen, and so on.

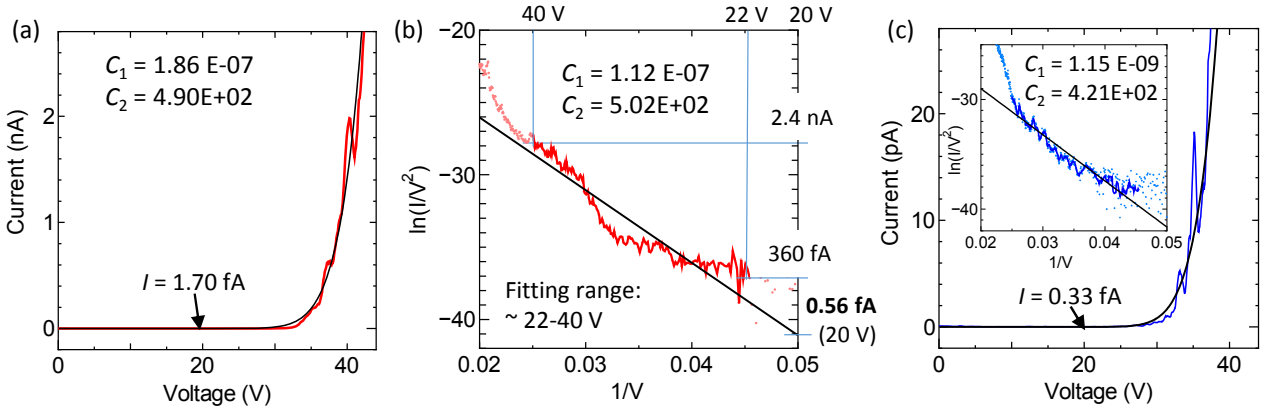

Figure S7. (a) Fitting line for the experimental *I-V* characteristic [in red in Figure 3(c)] with the FN law [$I = C_1V^2\exp(-C_2/V)$]. (b) Similar fitting for the FN plots for the same gap. Since the gap was extended by bias voltage of V = 20 V, these fittings yield the threshold current for gap extension in air of I = 0.56 – 1.70 fA. (c) The same fitting was applied to the gap drawn in blue in Figure 3(e). This gap yields the threshold current of I = 0.33 fA.

7. Strategy for full length and selective etching of m-SWNTs utilizing field emission

Site-controlled formation of gaps of m-SWNTs and s-SWNTs could be used for selective elimination of m-SWNTs in full length. A possible process is shown in Figure S8. Breakdown position of m-SWNTs can be easily controlled by depositing intermediate electrodes (drawn in gray in Figure S8b). The intermediate electrodes are selectively etched after the gap formation in m-SWNTs. Then,

site-selective cutting of s-SWNTs can be done, for example, by passivating large area of channel region to protect SWNTs from oxygen, except for near anodes (Figure S8c). After removing passivation layers, high voltage is applied in wet gas ambient (Figure S8d). All m-SWNTs can be removed in full length, as long as inter-SWNT spacing is small enough (Figure S8e). On the other hand, some m-SWNTs on anode side cannot be etched if the SWNT density is too small (Figures S8f and g).

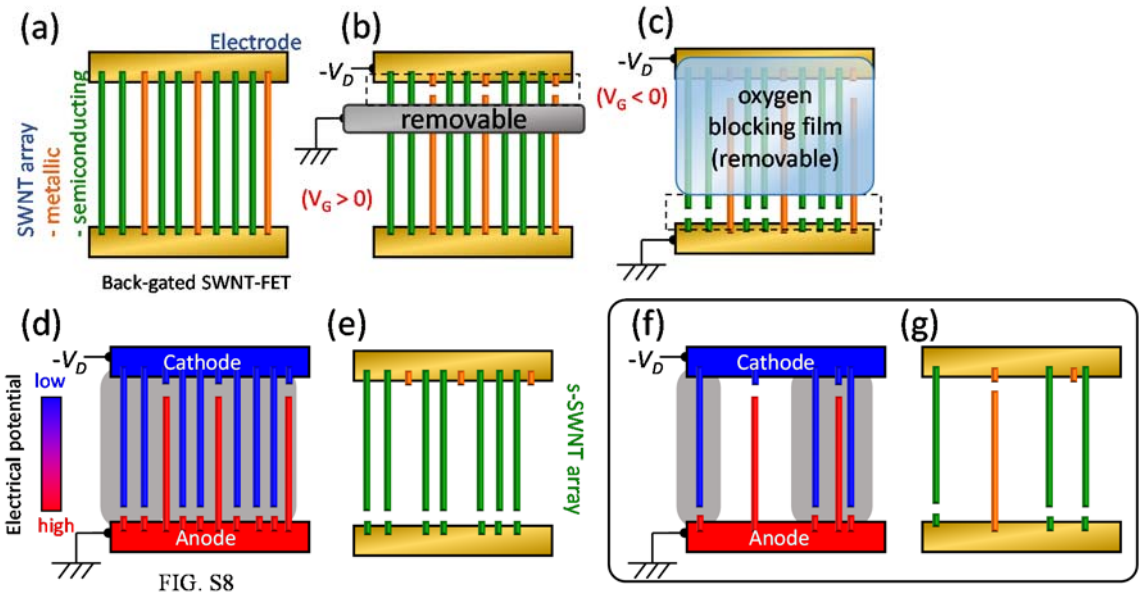

Figure S8. Schematic illustration of the potential application of A-SWNT etching by side walls of adjacent C-SWNTs. (a) Initial SWNT arrays. (b) Electrical breakdown of m-SWNTs near cathodes, and (c) following breakdown of s-SWNTs near anodes while voltage-driven etching is suppressed. (d) High voltage application to etch A-SWNTs (supposedly m-SWNTs) under wet gas condition. (e) s-SWNT arrays. (f,g) If the density of SWNT arrays is small, some A-SWNTs cannot be removed.

References

1 A. D. Liao, R. Alizadegan, Z.-Y. Ong, S. Dutta, F. Xiong, K. J. Hsia and E. Pop, *Phys. Rev. B*, 2010, **82**, 205406.

2 R. C. Smith, D. C. Cox and S. R. P. Silva, *Appl. Phys. Lett.*, 2005, **87**, 103112.

3 C. J. Edgcombe and U. Valdrè, *J. Microsc.*, 2001, **203**, 188–194.

4 J.-M. Bonard, K. Dean, B. Coll and C. Klinke, *Phys. Rev. Lett.*, 2002, **89**, 197602.